Review article

Daniel Pérez, Ivana Gasulla and José Capmany*

Programmable multifunctional integrated nanophotonics

Abstract: Programmable multifunctional integrated nanophotonics (PMIN) is a new paradigm that aims at designing common integrated optical hardware configurations, which by suitable programming can implement a variety of functionalities that can be elaborated for basic or more complex operations in many application fields. The interest in PMIN is driven by the surge of a considerable number of emerging applications in the fields of telecommunications, quantum information processing, sensing and neurophotonics that will be calling for flexible, reconfigurable, low-cost, compact and low-power-consuming devices, much in the same way as how field programmable gate array (FPGA) devices operate in electronics. The success of PMIN relies on the research into suitable interconnection hardware architectures that can offer a very high spatial regularity as well as the possibility of independently setting (with a very low power consumption) the interconnection state of each connecting element. Integrated waveguide meshes provide regular and periodic geometries, formed by replicating a unit cell, which can take the form of a square, hexagon or triangle, among other configurations. Each side of the cell is formed by two integrated waveguides connected by means of a Mach-Zehnder interferometer (MZI) or a tunable directional coupler that can be operated by means of an output control signal as a crossbar switch or as a variable coupler with independent power division ratio and phase shift. In this paper, we review the recent advances reported in the field of PMIN and, especially, in those based on integrated photonic waveguide meshes, both from the theoretical as well as from the experimental point of view. We pay special attention to outlining the design principles, material platforms, synthesis algorithms and practical constraints of these structures and discuss their applicability to different fields.

Keywords: integrated optics; nanophotonics; optical signal processing.

1 Introduction

Programmable multifunctional nanophotonics (PMIN) [1–15] is a new paradigm that aims at designing common integrated optical hardware configurations, which by suitable programming can implement a variety of functionalities that, in turn, can be exploited as basic operations in many application fields. Programmability enables by means of external control signals both chip reconfiguration for multifunction operation as well as chip stabilization against non-ideal operation due to fluctuations in environmental conditions and fabrication errors. Programming also allows the activation of parts of the chip, which are not essential for the implementation of a given functionality but can be of help in reducing noise levels through the diversion of undesired reflections. PMIN is therefore a transversal concept inspired by similar approaches, which are already employed in other technology fields. For instance in electronics, field programmable gate array (FPGA) devices enable a much more flexible universal operation as compared to application specific integrated circuits (ASICs). In communications, software defined networks (SDN) enable the exploitation and reconfiguration of a common set of resources provided by a network hardware infrastructure to ensure an optimum configuration in demand of time-varying requirements set upon several quality and bandwidth performance indicators. Finally, in wireless transmission, software radio (SR) allows the emulation of different specific radiofrequency receivers with a single hardware platform. In the area of photonics, the PMIN approach aims to provide a complementary approach to that based on application specific integrated photonics circuits (ASPICs). The objective is

*Corresponding author: José Capmany, Photonics Research Laboratories, ITEAM Research Institute, Universitat Politècnica de València, Camino de Vera s/n, 46022 Valencia, Spain,
e-mail: jcapmany@iteam.upv.es. http://orcid.org/0000-0002-6460-4167
Daniel Pérez and Ivana Gasulla: Photonics Research Laboratories, ITEAM Research Institute, Universitat Politècnica de València, Camino de Vera s/n, 46022 Valencia, Spain

Table 1: Basic features of ASIC and FPGA approaches in electronics.

	ASIC	FPGA
Time to market	Slow	Fast
Non-recurring engineering	Very high	Low
Unit cost	Low	Medium
Design flow	Complex	Simple
Performance	High	Medium
Application flexibility/versatility	Very low	High
Power consumption	Low	High
Size	Low	Medium

to leverage on the universal properties of this approach and seek similar advantages as FPGAs bring over ASICs in electronics as listed in Table 1.

PMIN has recently raised the interest of many research groups worldwide, justified by the surge of a number of emerging applications that are and will be calling for true flexibility, reconfigurability as well as low-cost, compact and low-power-consuming devices. One area in which considerable seminal work has been produced is in quantum information technologies, where PMIN can open avenues to large-scale quantum gates and boson sampling circuits based on unitary matrix transformations [1, 2, 5, 7]. In particular, quantum circuits have been developed based on the triangular multiport interferometer concept proposed by Reck et al. [13] and subsequently developed for integrated optics by Miller [3, 4] as well as from the more recent rectangular multiport interferometer proposed by Clements and co-workers [14, 15]. Unitary matrix transformations are also at the heart of reconfigurable neurophotonic systems and Fourier-based optical signal processors [16]. In the field of telecommunications, PMIN can be instrumental in a series of functionalities, such as the implementation of arbitrary mode converters [17, 18], fiber-wireless interfacing devices [19] and broadband switches [20], which can also form the basis for computer interconnection [21]. In the field of sensing, PMIN can lead to a generic class of programmable measuring devices [22], which might be successfully integrated as a building block in the future Internet of Things (IoT). All in all, the success of PMIN relies on the research of a suitable interconnection hardware architecture that can offer a very high spatial regularity as well as the possibility of independently setting (with a very low power consumption) the interconnection state of each connecting element. Integrated waveguide meshes [9–12] provide regular and periodic geometries, formed by replicating a unit cell, which can take the form of a square, hexagon or triangle, among other configurations. Each side of the cell is formed by two integrated waveguides connected by

means of a beamsplitter/tunable coupler that can be operated by means of an output control signal as a crossbar switch or as a variable coupler with independent power division ratio and phase shift. A mesh formed by a suitable amount of unit cells can be programmed to implement a wide variety of functionalities much in the same way as an FPGA operates in electronics [9, 12].

This paper reviews the recent advances reported in the field of integrated photonic waveguide meshes, both from the theoretical as well as from the experimental point of view. Section 2 provides a review of the integrated waveguide mesh concept including the description of its basic configuration element, the tunable basic unit (TBU), which is implemented by means of a beamsplitter/tunable coupler and we show how TBUs can be programmed to operate in a cross/bar state or as a tunable coupling device providing independent amplitude and phase values. In Section 3, we address how waveguide meshes can be programmed to implement both traditional signal processing structures, such as finite and infinite impulse response filters, delay lines, beamforming networks, as well as more advanced linear matrix optics functionalities. Section 4 discusses some experimental results reported both in silicon and silicon nitride material platforms and outlines some of the practical challenges to be overcome in future designs. In Section 5, we provide the main programming algorithms to implement these structures; in particular, some detailed discussion on the algorithms that can be programmed to implement arbitrary matrix transformations between the input and output waveguide ports and discuss their applications either as stand-alone systems or as part of more elaborate subsystems in microwave photonics, quantum information, optical signal processing and machine learning. Finally, Section 6 provides a summary wrap-up, the conclusions and directions for future work.

2 Nanophotonic integrated waveguide meshes (NIWMs)

2.1 Basic concept

2D integrated waveguide meshes are structures where a unitary TBU is spatially replicated to create cells [4, 9–14, 23]. Several examples are shown in Figure 1.

Each unitary cell is implemented by one or more sets of integrated waveguide pairs coupled by means of a TBU, the core of which can be either a balanced MZI or a directional coupler. The application of external electrical signals to the TBU allows the independent amplitude and
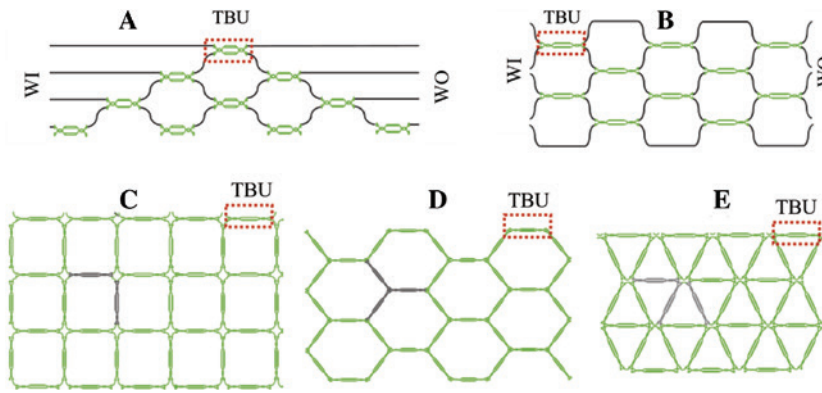
Figure 1: Different arrangements of beamsplitters to implement integrated waveguide meshes.
(A) Triangular feedforward proposed by Reck et al. [13] and reformulated by Miller [4], (B) rectangular feedforward proposed by Clements et al. [14], (C) squared feedforward/backward [9], (D) hexagonal feedforward/backward [10, 23] and (D) triangular feedforward/backward [10, 23]. WI/WO, waveguide inputs/outputs.

phase control of the photonic signals coupled between the two waveguides. In particular, each TBU in the mesh can be configured to operate either as an optical crossbar switch or as an intermediate power divider. In this way, the combination of different TBUs in the 2D grid – each individually configured as desired – enables the synthesis of any kind of optical core circuit topology, including finite (FIR) and infinite impulse response (IIR) multiport interferometers and filters. Figure 1A, B corresponds to meshes representing the triangular interferometer proposed by Reck et al. [13] and rectangular interferometer proposed by Clements et al. [14], respectively. In these, which have been widely employed in the implementation of quantum circuits [1–7], the unit cell is a single TBU. Note that they allow only feedforward propagation of light so they are limited to the implementation of FIR multiport interferometer filters. Figure 1C–E shows the main reported designs for waveguide meshes allowing for both feedforward and feedbackward propagation. Here the unit cell is composed by several TBUs following a geometrical configuration: *square*, *hexagonal* and *triangular*, respectively. These are the most flexible waveguide mesh configurations allowing the implementation of both FIR and IIR multiport interferometers and filters. Although each mesh topology has inherent advantages, recent studies have proved the hexagonal mesh is potentially the most flexible approach for implementing the PMIN concept.

2.2 Tunable basic unit (TBU) implementations

The central basic element in the waveguide mesh is the TBU [4, 9, 10, 13, 14]. Figure 2A shows an example of a hexagonal cell implemented by nine TBUs arranged in three trilattice structures. Each TBU can be programmed
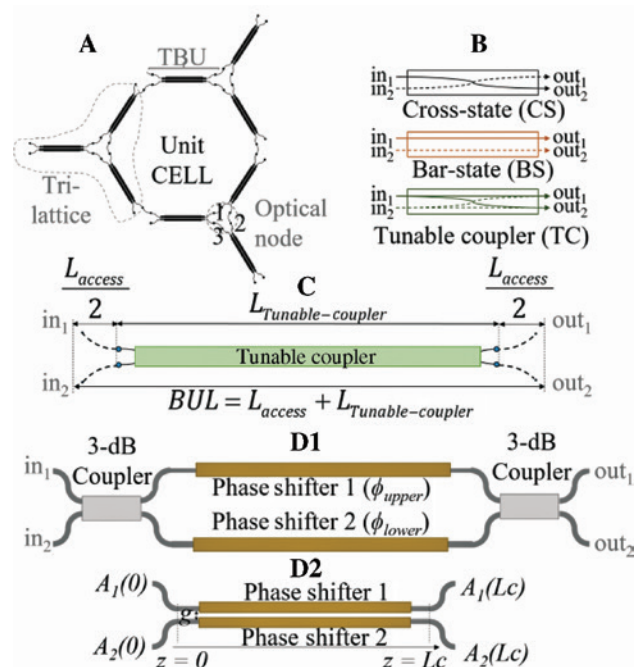

Figure 2: Single hexagonal cell implemented using three trilattices and alternatives for the tunable coupler unit.
(A) Hexagonal unit cell. (B) Signal flow for the different TBU configurations. (C) Schematic of a general tunable coupler acting as the basic building block of the mesh: tunable basic unit (TBU). The basic unit length is illustrated as the sum of the tunable coupler length and the arc length of the access waveguides. A particular case of a tunable coupler implemented by (D1) a MZI and (D2) an integrated dual-drive tunable directional coupler.

to operate in one of the three modes shown in Figure 2B. The central element of the TBU shown in Figure 2C is the tunable coupler, which can be implemented either by a balanced MZI [Figure 2D(1)] or by a dual drive directional coupler [Figure 2D(2)] [24].

2.3 TBU programming

Both MZI and dual drive-based TBUs can be programmed to achieve independent amplitude and phase shift settings. Here we illustrate the process for the MZI approach, but the reader can find detailed information regarding the dual drive directional coupler approach in Ref. [24]. Referring to Figure 2D(1), the TBU can be programmed, as mentioned, to implement three different states: cross state switch (light path connects in_1 to out_2 and in_2 to out_1), bar state switch (light path connects in_1 to out_1 and in_2 to out_2) and tunable splitter. For a balanced MZI loaded with heaters on both arms, the splitting ratio is obtained by increasing the effective index due to the Joule effect in the upper or lower arm, producing a ϕ_{upper} and ϕ_{lower} phase shift, respectively. Once set, a common drive in both heaters will provide a common phase shift, leading to independent control of the amplitude ratio and the phase. The device matrix is defined by [4, 15]:

$$h_{TBU} = je^{j\Delta}\begin{pmatrix} \sin\theta & \cos\theta \\ \cos\theta & -\sin\theta \end{pmatrix}\gamma, \quad (1)$$

where, θ is $(\phi_{upper} - \phi_{lower})/2$ and Δ is $(\phi_{upper} + \phi_{lower})/2$. The coupling factor K is then defined as $\cos^2(\theta)$. Finally, γ is a general loss term that includes the propagation and insertion losses of the access and tunable coupler waveguides and the 3-dB couplers, respectively. For practical applications and in the case of MZI-based TBUs, a more detailed description of the TBU operation is desired that takes into account the departure from the ideal 3 dB splitting ratio of the input and output couplers in the MZI, and the uneven insertion losses in each of its arms. This matrix representation has been derived by Mower and co-workers in Ref. [25] and then applied in conjunction with random phase statistical representations of θ and Δ to analyze the impact of imperfect TBUs over the fidelity of several quantum gate circuits and the impact that their reconfigurability brings in improving this figure of merit. Indeed, TBU reconfigurability brings the additional potential for correcting fabrication errors and demonstrations have been also reported over classical circuit configurations [6, 12].

3 Operation modes

3.1 Waveguide mesh allocation in PMIN processor

While the 2D waveguide mesh is the key central element required in PMIN, there are other components that are needed to configure a programmable processor [19, 23]. The left part of Figure 3 represents the general photonic processor architecture for a wide range of applications.

All the elements are connected to the 2D reconfigurable photonic integrated waveguide mesh in such a way that they produce the desired processing engines as well as dynamically connect the internal and the external elements required for different functionalities. The processor includes, as shown, both passive and active photonic components, interface ports with electronic control signals and RF driving input and output ports. Also, pure input/output optical ports can be directly accessed.

The right part of Figure 3 illustrates a possible design based on a hybrid design approach. In this case, the low-loss silicon passive platform (ochre colour) is chosen to implement the passive devices, while indium phosphide (red colour) is used for the active devices. Note that an array of optical amplifiers in this platform might be required to overcome the large conversion losses when moving from the radiofrequency to the optical domain. These losses are mainly related to the conversion efficiency of modulators and photodetectors as well as the propagation losses.
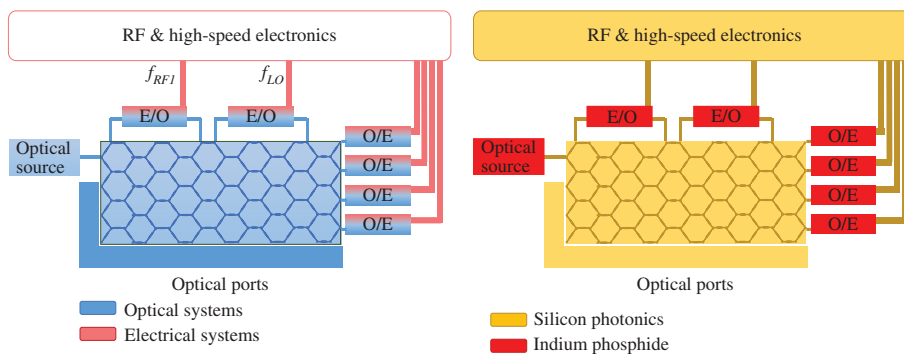

Figure 3: High level configuration of a general photonic integrated processor including passive and active components.
(Left) General photonic integrated processor architecture and (right) candidate fabrication platforms for each subsystem (after Ref. [23]).
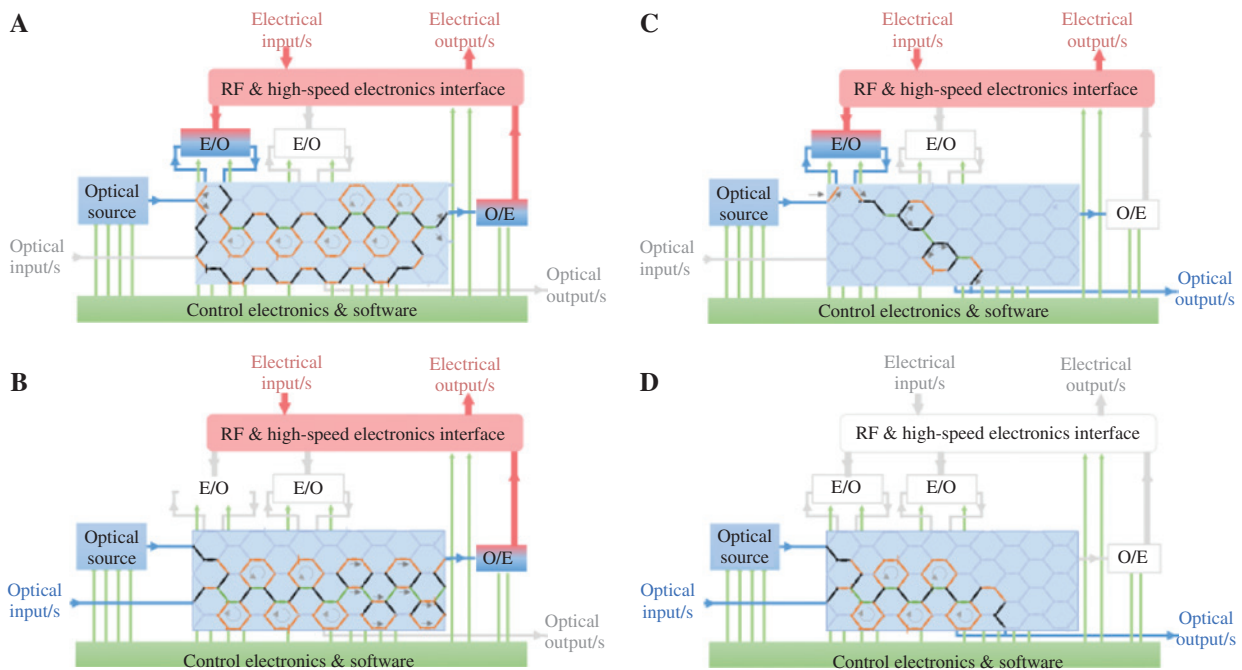
Figure 4: The four different alternatives for the operation modes of programmable multifunctional nanophotonics processor. (A) Electrical input/electrical output, (B) electrical input/optical output, (C) optical input/electrical output and (D) optical/optical.

Optical amplifiers should also be implemented in InP and their optimum allocation is under current research. The recent development of InP device stamping techniques [26] and InP membranes on Silicon [27] opens the path for the compact and versatile implementation of this required hybrid integration approach.

3.2 Operation modes for the PMIN processor

The processor architecture supports four different modes of operation as far as the input/output signals are concerned: electrical/electrical, electrical/optical, optical/electrical and optical/optical operations. These are illustrated in Figure 4.

Electrical/electrical operations are typically employed in microwave photonic (MWP) functionalities such as reconfigurable radiofrequency (RF) filtering, instantaneous frequency measurement, frequency mixing, RF and millimeter-wave arbitrary signal generation to cite a few. It requires the processor to enable an optical source, electro-optic (EO) and optoelectronic (OE) converters as well as the reconfigurable optical core. Figure 4A illustrates the signal flow for these operations. Note that if a second modulator is integrated, it can be enabled to perform frequency mixing operations based on the cascade of two EO modulators. Sometimes, the processed signal has to be distributed over a particular fiber link length after

generation and/or processing. The processor can leverage the inherent properties of optical fibers for distribution purposes. The electrical/optical mode is widely employed in radio-over-fiber MWP links. At the receiver point of the link, another multipurpose MWP processor can be employed. In this case, the receiver would be working in optical/electrical mode, processing the signal before the photo-detection. Optionally, the receiver can enable its own optical source to act as a local oscillator as well. Both modes of operation are displayed in Figure 4B and C, respectively. The last mode of operation, illustrated in Figure 4D, is the optical/optical. In this case, the input signal can be processed directly in the optical domain. Optical channel management can then perform common optical processing operations such as add/drop, switching and broadcasting. Note that all the previous modes of operation may coexist for a certain multi-task functionality. For example, a modulated signal could be divided after being processed and both distributed through the optical ports and down-converted by the photodetectors.

3.3 Single-input/single-output and 2×2 circuit programming

The 2D integrated waveguide mesh can be programmed to operate as a standard single input/single output (SISO) or a 2×2 signal processor [9, 10, 12]. In principle,
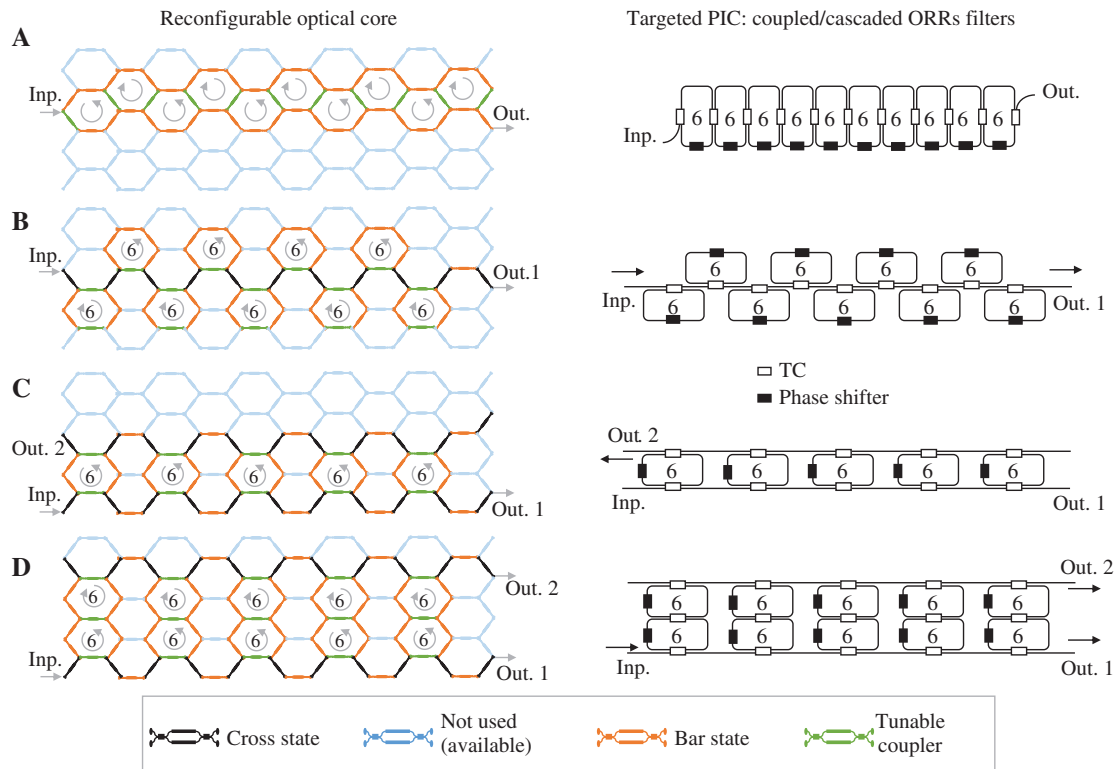
Figure 5: Different examples of programming different single input-single outtput and 2×2 circuits using the same waveguide mesh and resulting circuit layouts.
(Left) Settings for CROW and SCISSOR filter implementations in the hexagonal mesh core for (right) (A) 10th-order CROW, (B) 9th-order single channel SCISSOR, (C) 5th-order double channel SCISSOR and (D) twisted double channel SCISSOR. 6-BUL cavities are specified.

it has been demonstrated that internal connections set by proper biasing of the intermediate TBUs can enable the programming of a wide variety of functionalities including: finite impulse response (FIR) filtering implemented either by 2×2 unbalanced MZI lattice structures and transversal filters, infinite impulse response (IIR) filters including single and multi-cavity resonators and more complex hybrid structures such as coupled resonator optical waveguides (CROWs) and side-coupled integrated spaced sequence of resonators (SCISSORs). Adequate programming also allows the implementation of tunable true time delay lines. As an example, Figure 5 shows the settings and programming of a hexagonal 2D integrated waveguide mesh to provide different CROW and SCISSOR structures [12]. Here, each cavity is defined by six TBUs, setting the free spectral range.

3.4 Multiple-input/multiple-output and M×N matrix transformer programming

A second and probably more versatile mode of operation is as a multiple input/multiple output (MIMO) processor

that implements an arbitrary unitary transformation. In essence, this task is equivalent to that of a linear optics device, which transforms a series of N orthogonal modes ($|\phi_I\rangle$) into the corresponding N orthogonal modes at the output ($|\phi_O\rangle$) [3, 4, 15]. This transformation is defined by means of a unitary matrix U ($|\phi_O\rangle = U|\phi_I\rangle$). Linear transformations are the fundamental building block of many applications in quantum information and communication systems, switching and routing, microwave photonics and optical channel management and supervision. The 2D hexagonal integrated waveguide mesh enables the implementation of the two layout versions of the universal linear interferometer proposed in the literature. The first case corresponds to a Reck-Miller triangular arrangement interferometer [13]. Figure 6A displays an example of a 4×4 interferometer implemented by means of a triangular arrangement of beamsplitters and Figure 6B shows the equivalent structure implemented on a hexagonal waveguide mesh. Each beamsplitter can set a certain splitting ratio and a relative phase to the upper output. Reck et al. and Miller have developed algorithms to program and configure the triangular arrangement, so it can implement any desired linear unitary
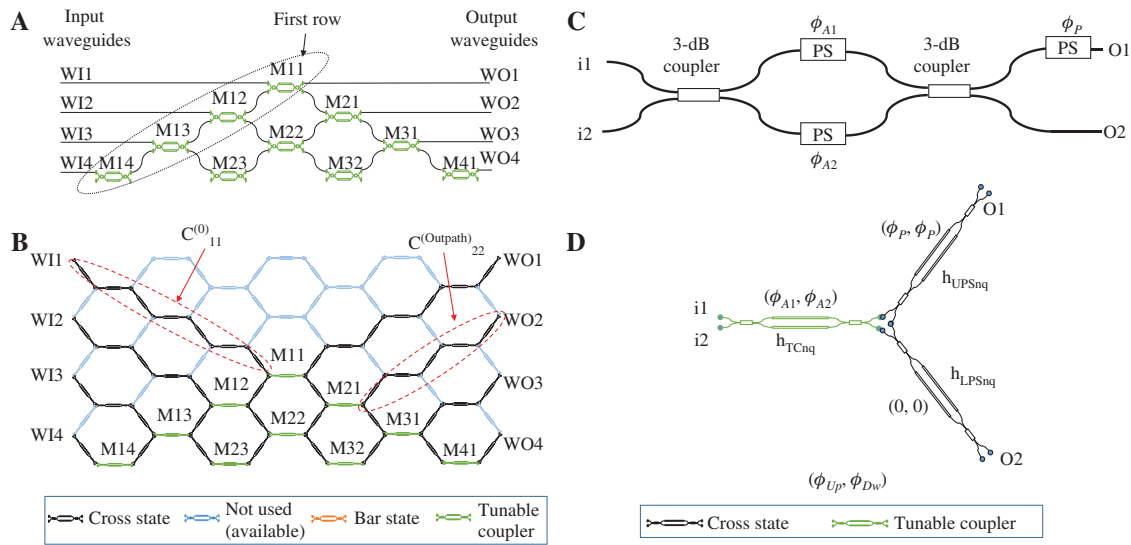
Figure 6: Layout and emulation using the hexagonal waveguide mesh of a triangular 4×4 universal interferometer.
(A) Classical triangular arrangement and (B) hexagonal mesh-based implementation of a 4×4 interferometer. (C) Beamsplitter for the classical approach and (D) corresponding beamspliter implementation with three TBUs for the hexagonal waveguide mesh.

transformation [13]. To adapt, for example, the synthesis algorithm developed by Miller to the hexagonal waveguide mesh we, first of all, need to consider the possible different phase contributions due to the different access paths established between the interferometer inputs and the internal processing elements forming the triangular arrangement of beam splitters and, from these, to the different outputs.

These different phase contributions must be compensated. Then, we need to establish an equivalent configuration – using the available elements in our hexagonal waveguide mesh – to the MZI with a phase shifter in the upper output port employed by Miller and shown in Figure 6C. In our case, as illustrated in Figure 6D, the equivalent "beamsplitter" is implemented using a TBU for the tunable coupler [with a transfer matrix defined by
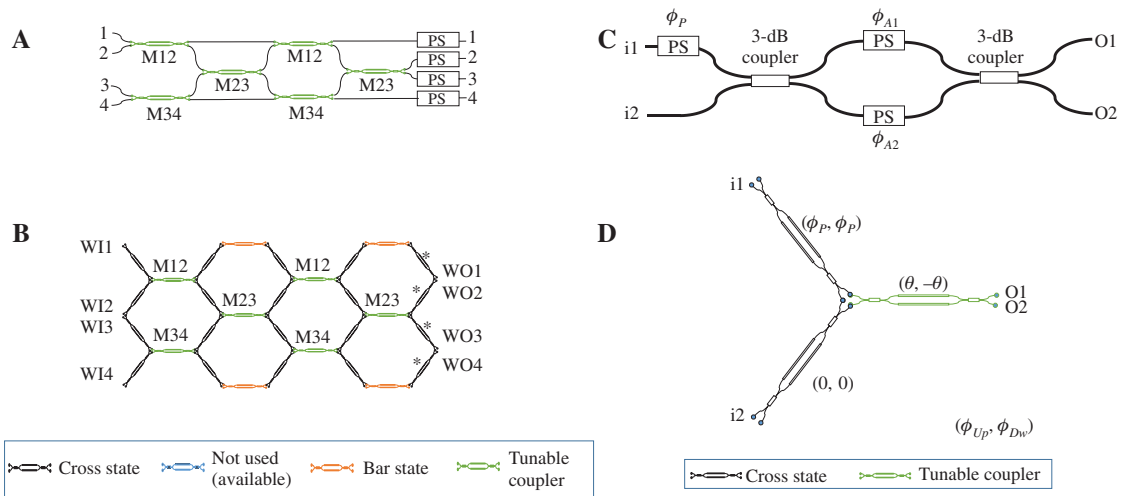

Figure 7: Layout and emulation using the hexagonal waveguide mesh of a rectangular 4×4 interferometer.
(A) Rectangular arrangement of a 4×4 interferometer and (B) equivalent implementation using the hexagonal waveguide mesh. (C) MZI and phase shifter arrangement proposed in Ref. [14] for the implementation of the beam splitters in the rectangular arrangement. (D) Equivalent configuration for the MZI and phase shifter arrangement using the elements available in the hexagonal cell. (φ_{Up}, φ_{Dw}) are the upper and lower phase shift applied to each TBU arm.

h_{TC} as in Eq. (1)], followed by two TBUs, which are biased in cross state and employed as output connections. In the latter, the upper TBU also implements a phase shifter and is defined by the transfer matrix h_{UPS}. The lower TBU is defined by the transfer matrix h_{LPS}. Miller's synthesis algorithm is based on writing any of the input basis functions as a linear combination of each input port or rectangular functions ($|\phi_{In}\rangle$), and configuring sequentially each row of beam couplers for each input mode. These input modes can be obtained from the columns of the Hermitian Adjoint of the matrix U. A procedure describing the synthesis algorithm adaptation is discussed in Section 5. The novel multiport interferometer configuration based on a rectangular arrangement proposed by Clements et al. [14] can also be emulated using the hexagonal 2D integrated waveguide mesh. Figure 7A displays an example illustrating the implementation of a 4×4 multiport interferometer. Figure 7B shows the equivalent structure implemented on a hexagonal waveguide mesh. In the algorithm developed by Clements et al. [14], each beamsplitter (Figure 7C) sets a certain splitting ratio and a relative phase sequentially to program and configure the whole rectangular arrangement so it can implement any desired linear unitary transformation efficiently.

4 Fabrication technologies and salient experimental results

4.1 Reported waveguide meshes in silicon photonics

Silicon photonics is one of the most attractive integration platform for programmable waveguide meshes since it allows high-volume fabrication as well as high integration densities due to its low refractive index contrast and moderate propagation losses among 0.5–2.5 dB/cm.

Silicon feedforward waveguide meshes have been reported for the implementation of mode conversion operations [18, 19]. In Ref. [18], Ribeiro and co-workers reported the implementation and demonstration of a 4×4-port universal linear optical circuit based on a triangular multiport interferometer arrangement [13], where the silicon photonic circuit, combined with electronic control and software feedback can perform any linear operation between its input and output ports. The circuit, illustrated in Figure 8A, B, consisted of a network of thermally tunable symmetric Mach-Zehnder interferometers with phase and amplitude control, in-circuit
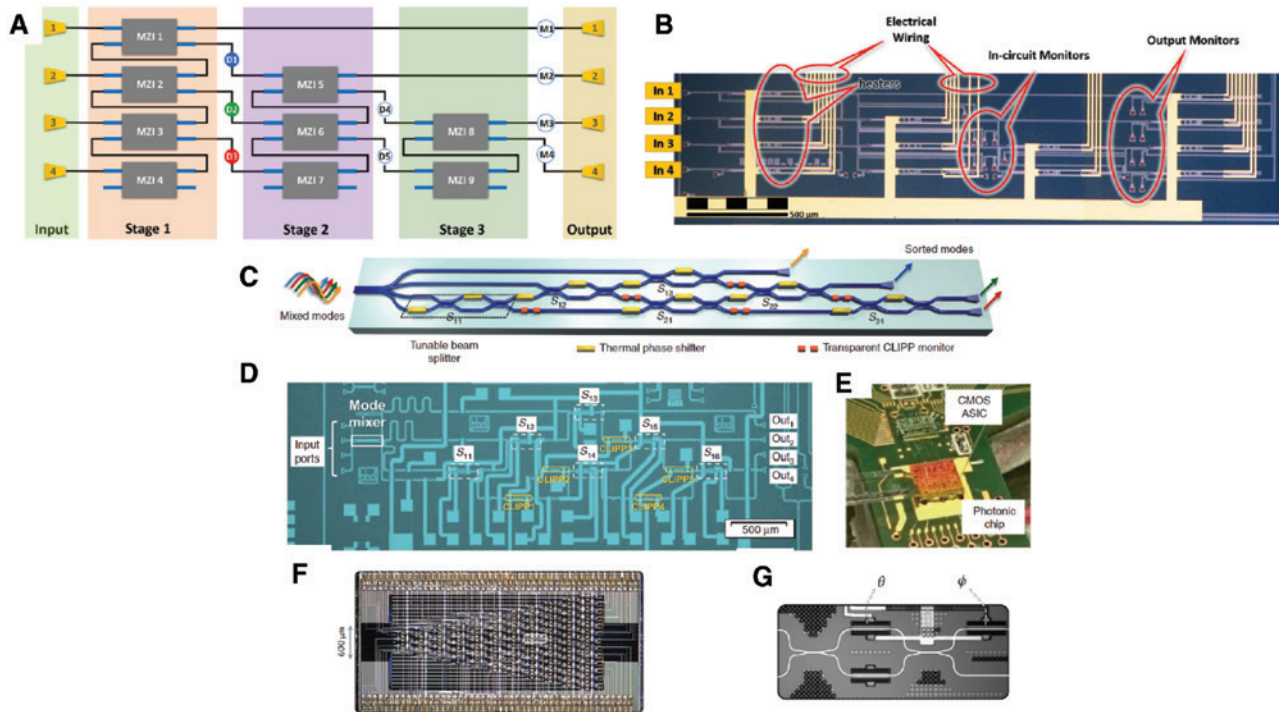

Figure 8: Different examples of reported silicon feedforward waveguide mesh circuits.
Schematic (A) and microscope image (B) of the integrated implementation of the mode converter circuit using MZIs after Ref. [18]. Guided-wave implementation (C), microscope image (D) and assembled carrier (E) of the mode unscrambler using MZIs reported in Ref. [19]. Processor composed of 88 MZIs, 26 input modes, 26 output modes and 176 phase shifters (F) reported in Ref. [28] and detail of the integrated beamplitters implemented using a 3-dB MZI (G).
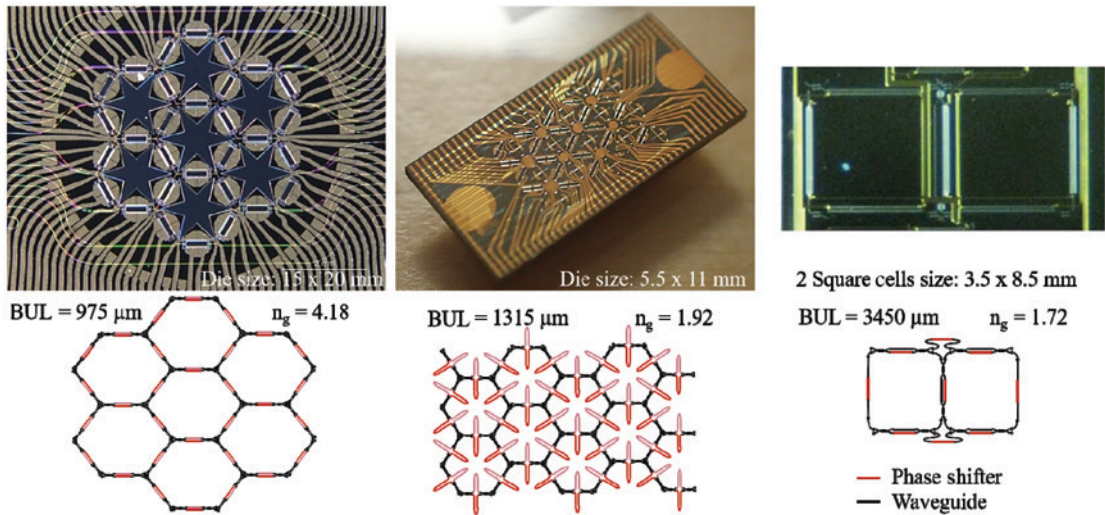
Figure 9: Chip picture and fabricated layout for different feedforward/backward waveguide meshes using different material platforms and cell geometries.
(A) Hexagonal topology in silicon [12], (B) hexagonal topology in Si_3N_4 with modified TBU scheme [29] and (C) square topology in Si_3N_4 [9].

optical power monitors, and local software-controlled feedback loops. More recently, Annoni and co-workers [19] have reported a 4×4 mode unscrambler based also on a triangular Reck multiport interferometer arrangement as shown in Figure 8C. The chip was able to automatically unscramble optical beams, which had been arbitrarily mixed in a multimode waveguide, undoing the scattering and mixing between the spatial modes. The structure incorporated a set of transparent light detectors integrated in a photonic chip as shown in Figure 8D that were used to directly monitor the evolution of each mode along the mesh and allowed sequential tuning and adaptive individual feedback control of each beam splitter. Electronic reconfiguration and setting-up was enalbled by an assorted Complementary Metal Oxide Semiconductor (CMOS) ASIC shown in Figure 8E. More recently, Harris and co-workers [28] have reported a reconfigurable chip built upon a waveguide mesh of integrated beamsplitters (see Figure 8F) implemented using integrated MZIs as shown in Figure 8G. The Chip includes 88 MZIs and 176 phase shifters and, by suitable programming of the latter, it has been employed to emulate over 64,000 different quantum particle and phase transport experiments.

Regarding feedforward/backward meshes, we recently reported the results of a waveguide mesh composed of 7 hexagonal cells (30 thermally tuned TBUs) fabricated in Silicon on Insulator. The chip photograph is shown in Figure 9A. The device was fabricated at the Southampton Nanofabrication Centre at the University of Southampton. Silicon on insulator (SOI) wafers with a 220-nm-thick silicon overlayer and a 3-µm-thick buried

oxide layer were used (for more details on fabrication and testing see [12]).

Despite the simplicity of the layout depicted in Figure 9A, the 7-cell structure is capable of implementing over 100 different circuits for MWP filtering applications (basic MZI, FIR transversal filters, basic tunable ring cavities and IIR filters, as well as compound structures such as CROWs and SCISSORs), true time delay lines and optical coherent interferometry. The basic delay was 13.5 ps, given by a BUL of 975 µm and a group index of 4.18.

4.2 Reported waveguide meshes in silicon nitride

Silicon nitride waveguide meshes benefit from the integration of low propagation losses waveguides between 0.00045 and 1.5 dB/cm with moderate integration density values. Figure 9C shows the basic layout and photograph of the programmable optical chip architecture connecting thermally tuned MZI devices in a square-shaped mesh network grid proposed by Zhuang and co-workers [9]. The structure, fabricated in Si_3N_4, comprised two square cells, was fully programmable and was employed to demonstrate simple FIR and IIR impulse response filters with single and/or double input/output ports of synthetized ORRs (see next subsection). We recently designed a mesh based on thermally tuned 40 TBUs which is shown in Figure 9B. In this case, we re-designed the shape of the TBU to achieve a more compact layout and increase the component integration density. This chip has been
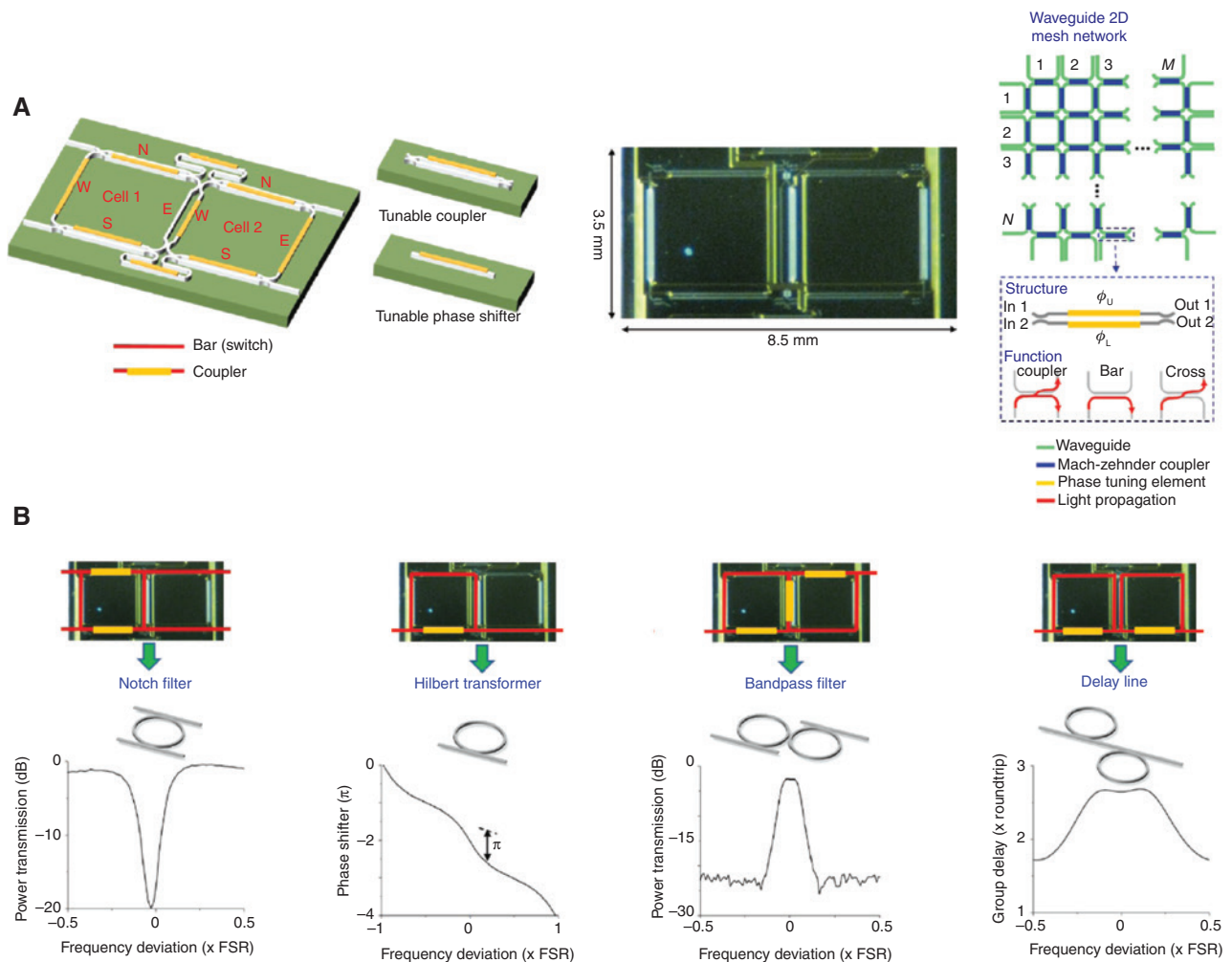
Figure 10: Programming and different circuit emulations using a two-cell square waveguide mesh in silicon nitride.
(A) Schematic and a photo of the Si$_3$N$_4$ waveguide technology (TriPleX) chip implementing a 2-square cell waveguide mesh reported in Ref. [9]. (B) Experimental results for different programmed circuit configurations obtained by varying phase-tuning elements in the chip and the measurements of their corresponding frequency responses.

fabricated in a Multi-Project Wafer run at a fabrication platform developed by VLC Photonics and the Centro Nacional de Microelectrónica (CNM) [29], and is currently under test. Based on previous and current fabrication runs, we expect a maximum Free Spectral Range (FSR) of 60 GHz, given by a basic time delay of 8.42 ps (group index of 1.92 and a BUL of 1315 μm).

4.3 Salient experimental results for feedforward/backward meshes

Figure 10A shows the basic layout and photograph of the programmable optical chip architecture connecting MZI devices in a square-shaped mesh network grid proposed by Zhuang and co-workers [9]. The structure, fabricated in Si$_3$N$_4$, comprised, as mentioned above, two square cells

and featured a FSR of 14 GHz. By appropriate programming of this processor, Zhuang et al. demonstrated bandpass filters with a tunable center frequency that spans two octaves (1.6–6 GHz) and a reconfigurable band shape (including flat-top resonance with up to passband-stopband 25-dB extinction). They also demonstrated notch filters with up to 55 dB rejection ratio, Hilbert transformers and tunable delay lines as shown in Figure 10B. The basic delay was greater than 19.7 ps, given by a BUL of 3450 μm and a group index of 1.72.

Regarding the hexagonal waveguide mesh circuit reported in Silicon, by suitably tuning the TBUs in the 7-cell hexagonal waveguide mesh, the authors were able to program a wide variety of PIC topologies and design parameters [12, 15]. For example, Figure 11 illustrates a single cavity optical ring resonator with a cavity length given by 6 BULs. The figure shows in (A) the waveguide
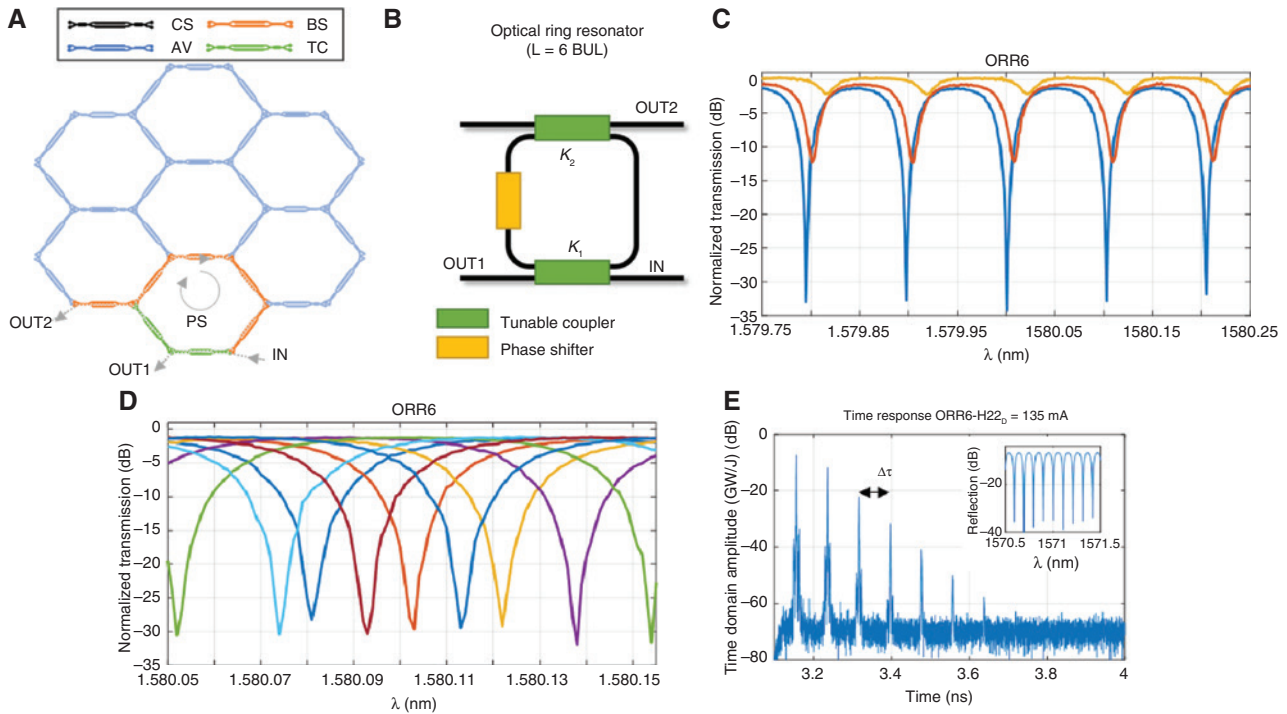
Figure 11: Experimental results for 6-BUL ring resonator IIR and FIR + IIR filters programmed over the silicon hexagonal waveguide mesh of Figure 9A.
(A) Waveguide mesh connection diagram, (B) circuit layout and (C) measured modulus transfer function for an IIR filter for different values of the coupling constants K_1 and K_2, (D) IIR filter along a full spectral period for different values of the optical ring resonator round-trip phase shift and (E) time response for critical coupling condition.

mesh configurations (with the TBU device status according to the colour code previously described), (B) the circuit layout and (C) the modulus response for the OUT_1 port. The measured results correspond to different values of K_1 and K_2, which settle the positions of the zero and the pole. The IIR filter tunability, which is shown in Figure 11D, is achieved by exploiting the fact that the coupling constant and the phase shift in any TBU of the mesh can be adjusted independently. Hence, any TBU inside the cavity can be operated as a constant-amplitude phase shifter. Finally, Figure 11E shows the time response of the ring resonator when the critical coupling is achieved.

More complex filter programming by incorporating more cavities and delay line paths could also be programmed over the same structure and are reported in Ref. [12]. For example, Figure 12 shows the results obtained when the mesh is programmed to implement double- and triple-cavity filters. Figure 12A illustrates a CROW structure where two cascaded ring resonators (input: IN, output: OUTPUT 1) implement a series of reconfigurable filters by arbitrarily moving its zeros and poles. One of the TBUs identified by an asterisk (*) was kept unbiased. Nevertheless, this is an example of how TBUs can be configured in order to extract non-ideal leaking due to optical crosstalk from the circuit. Figure 12B shows

the reflection response of two coupled ring resonators in a SCISSOR configuration (input: IN, output: OUTPUT 1). This circuit structure is widely used for dispersion compensation and reconfigurable filtering. Figure 12C shows the transmission response (input: IN, output: OUTPUT 2) of a CROW comprising three ring resonators.

Recently, the same configuration has been employed for the implementation of time-domain true time delay lines and assorted circuits [24]. The upper part of Figure 13 illustrates the programmed configuration of two discrete delay lines enabled by the hexagonal mesh featuring paths of 5 and 11 BULs, respectively. The lower part of the figure displays the measured results obtained by enabling different paths in a recently reported SOI chip where TBUs were implemented using 3-dB MZI-based TBUs.

Note that the amplitudes of the different delayed pulse replicas are different, which is due to the different losses experienced by the signal as it propagates through different paths. In particular, the logarithmic power response vs. length (time) was measured to be approximately linear with a decaying rate of 0.59 dB per BUL (per 13.5 ps). Errors in the fitting are mainly related to variations in grating coupler losses (±0.5 dB) and to a lesser extent in TBU losses (<0.1 dB) [12]. Note that different input/output port combinations
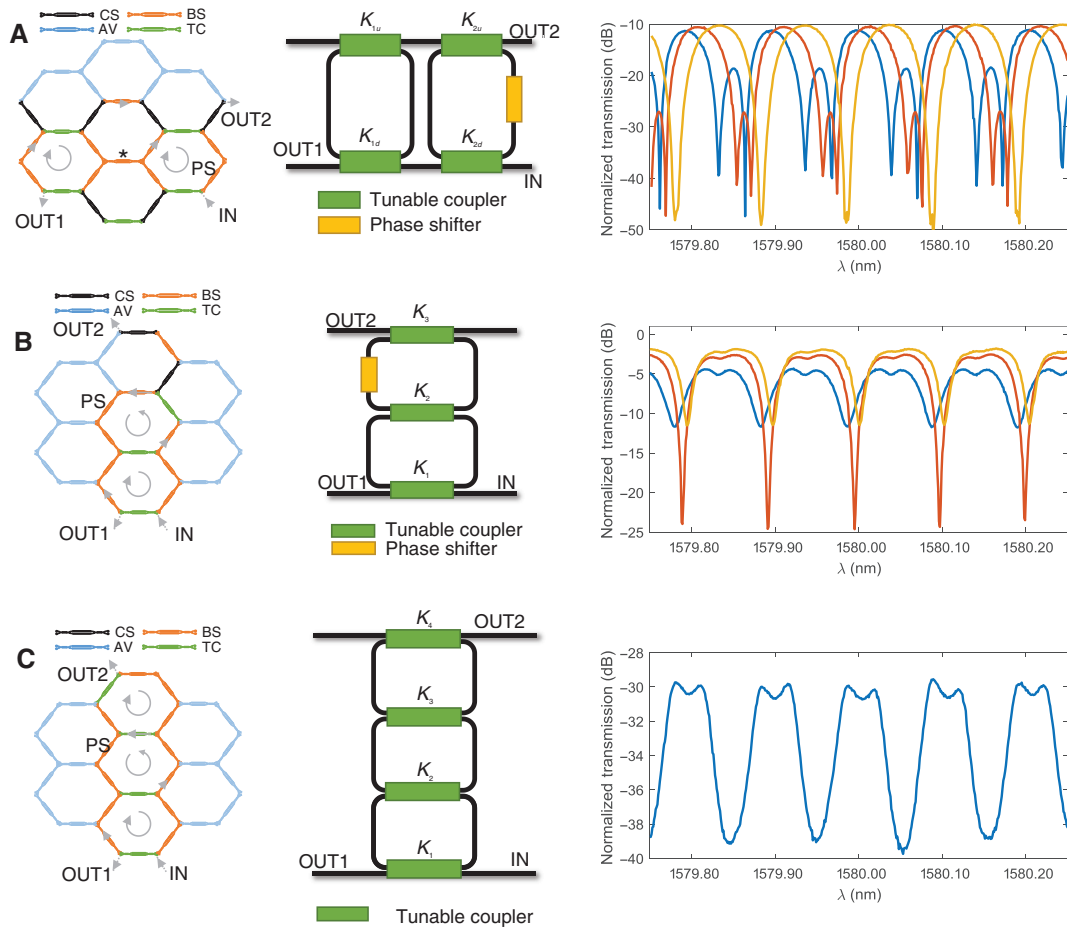
Figure 12: Experimental results for tuneable multicavity ring filters programmed over the silicon hexagonal waveguide mesh of Figure 9A. Waveguide mesh connection diagram (left), circuit layout (middle) and measured modulus (right) for different values of the coupling constants K_1 and K_2 in the case of (A), a 6-BUL side-coupled integrated spaced sequences of optical resonator (SCISSOR) filter; (B) a 6-BUL coupled resonator waveguide (CROW) filter; (C) a 6-BUL CROW. For each case, the first column shows the 7-cell hexagonal waveguide mesh configuration, where each Mach-Zehnder interferometer (MZI) device is represented by a given colour following the code given in Figure 5. The second column shows the layout of the implemented structure, while the third column shows the measured modulus for the synthesized configuration where the input is in the IN port and the outputs are the OUT1 and OUT2 ports. BUL, basic unit length; PS, phase shifter; CS, cross state; BS, bar state; AV, available; TC, tuneable coupler.

were employed. Nevertheless, these amplitudes can be equalized (though not shown in the figure) using the ability of TBUs to independently tune their coupling constant values if a splitting tree configuration is required.

Linear matrix transformations can be implemented either by feedforward-only waveguide meshes or by feedforward/backward designs. For instance, Figure 14 shows the measured 4×4 mode mixing matrix transformations implemented by the circuit reported by Anoni et al. [19]. After the mode mixing operation evenly distributing the powers of all the four modes among the four chip inputs by means of matrix H, the circuit was reconfigured to select different full mode sorting to different outputs according to different values of its tansformation H_{mesh}.

The hexagonal waveguide mesh chip could also be programmed for implementing several 3×3 and 4×4 linear

unitary transformations as reported in Ref. [17]. These are relevant examples of signal processing tasks that are needed in different applications. Figure 15 illustrates, for example, an experimental demonstration of a 3×3 linear unitary transformation corresponding to a three-way beamsplitter and a discrete Fourier transform (DFT) configuration. In all cases, the measured results show an excellent agreement with the targeted matrices for the operation wavelength of $\lambda = 1580$ nm with an extinction ratio >25 dB between the 1 and 0 coefficients. The required values for the coupling constants and phases of the TBUs used in these implementations were obtained by the synthesis algorithm adaptation explained in the next section. The resulting coefficients are translated into the required injected currents to the phase shifters according to the calibration curves obtained for each TBU during the chip characterization.
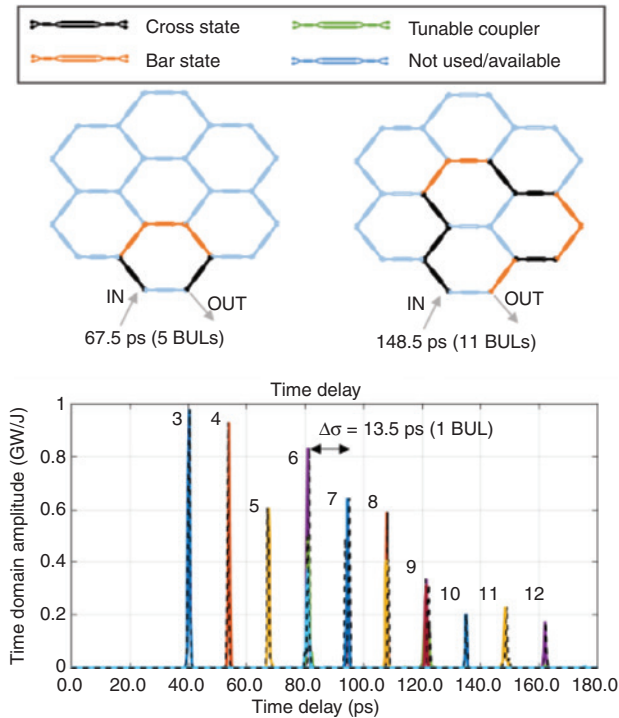
Figure 13: Discrete optical delay lines programmed over the silicon hexagonal waveguide mesh of Figure 9A.
(Up) Settings for two different time delays corresponding to 5 and 11 BULs, respectively. (Bottom) Measured delays up to 12 BULs (after Ref. [24]).

More complex 4×4 transformations were demonstrated including that corresponding to the C-NOT universal quantum gate as shown in Figure 16. Note again that the same waveguide mesh allows for a fast reconfiguration of these $N\times N$ transformers to perform different operations according to the synthesized values for their TBU parameters.

4.4 Practical limitations

Ideally, a higher number of TBUs results in a more versatile waveguide mesh circuit. However, in practice, there exist footprint limitations together with several sources of degradation that must be considered: accumulated losses, imperfect coupling splitting ratios, phase control, parasitic back-reflections, loss imbalances, fabrication errors (gradients through the circuit in thickness or temperature) and drift in time [19, 23].

Several works reporting the integration of a high-density MZI arrangement for matrix switching operations have succeeded at integrating more than 450 structures in a single die in a Silicon on Insulator platform, exceeding the Moore Law limits [30].

When designing programmable waveguide meshes, the designer faces an important miniaturization trade-off: minimum delay and accumulated losses. The BUL and the group index will determine the minimum delay. For low refractive index difference platforms, the BUL is mainly limited by the tuning mechanism length and the 3-dB coupler lengths. 3-dB couplers in silicon can be reduced to less than 50 μm [31, 32], including the bend sections while the heaters can be reduced to 62 μm [33]. With the inclusion of bends and straight waveguide sections to increase the distance between both arms of the TBU to decrease thermal crosstalk, a total BUL of 240 μm seems potentially achievable. Assuming a typical SOI group index of 4.18, this is translated to maximum FSRs of around 150 and 50 GHz for the synthesis of MZIs and ORRs, respectively, in the hexagonal waveguide mesh topology. However, a reduction of the BUL implies that the signal must go through a greater number of TBUs to obtain a desired delay. If the 3-dB couplers limit the overall IL of the TBU, this miniaturization trade-off must be highly considered. In fact, the main limitation of these structures resides in the number of accumulated losses. Assuming 0.1-dB loss 3-dB couplers, a path equivalent to 50 BULs will experience additional 10-dB losses than a classic waveguide of the same length.

Finally, the tuning mechanism impact on the final TBU length, tuning crosstalk and power consumption will limit the maximum number of active TBUs at the operational mesh and its performance. The use of alternative tuning mechanisms MEMS, piezoelectrics or electromechanics are promising solutions to reduce the power consumption while enabling a reduction of the distance between the two TBU arms.

5 Circuit emulation, synthesis and programming

5.1 Circuit emulation capability

PMIN processors can directly implement and/or emulate a variety of circuit classes. Table 2 summarizes the main features for both the feedforward-only and feedforward/backward configurations.

From Table 1, it follows that feedforward/backward configuration provides the highest operation flexibility and thus, in the following, we describe the synthesis procedures for this option.
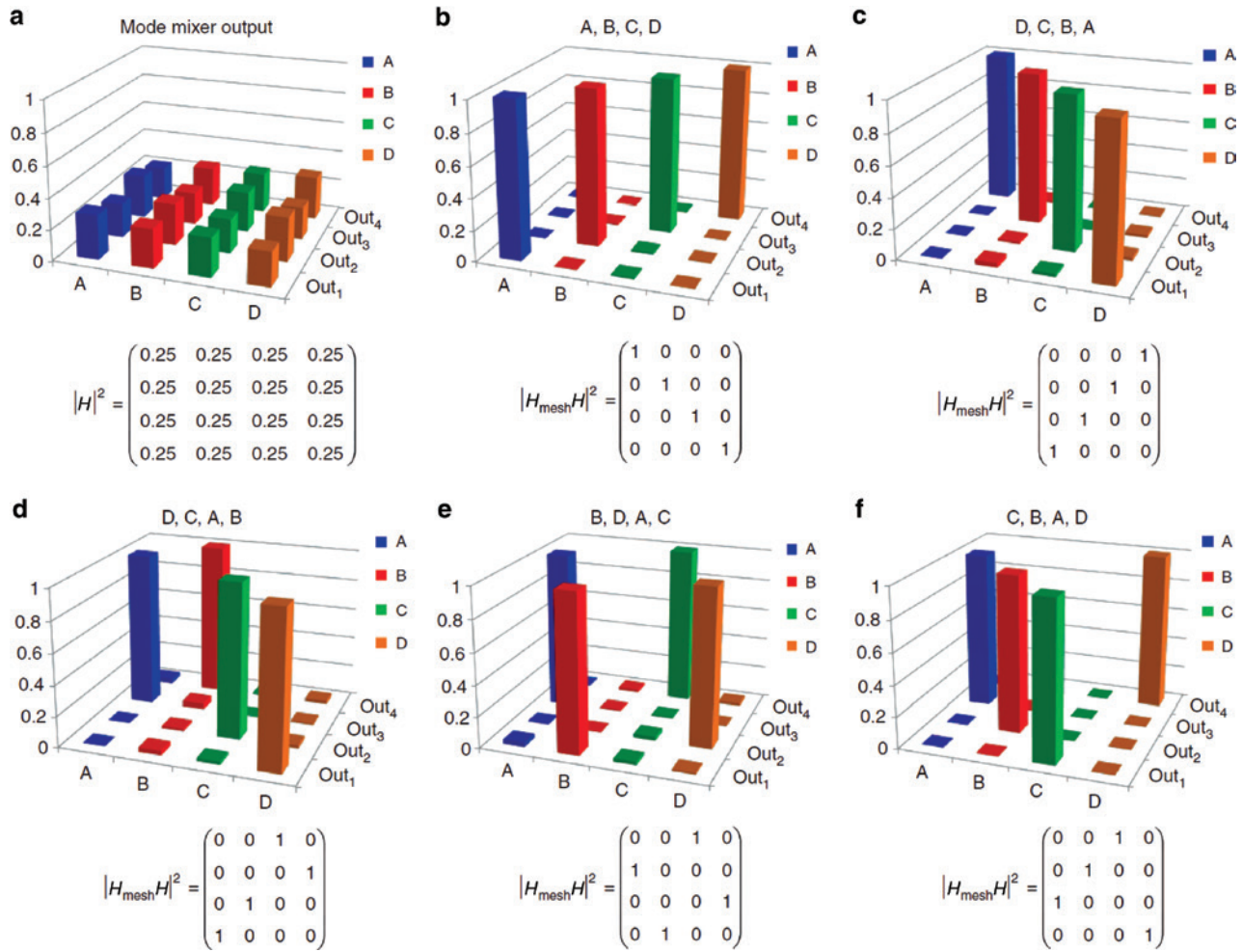
Figure 14: On-chip mode sorting operation of a 4×4 feedforward-only 4×4 chip reported in Ref. [18].
The mesh transmission matrix H_{mesh} can be configured in order to sort the reconstructed modes {A, B, C, D} arbitrarily at the output ports {Out1, Out2, Out3, Out4} of the mesh after mode scrambling by mode mixer H, evenly spreading the power in the input waveguides of the mesh (a), (b–f) different sorting configurations (b) A, B, C, D; (c) D, C, B, A; (d) D, C, B, A; (e) C, A, D, B; and (f) C, B, A, D.
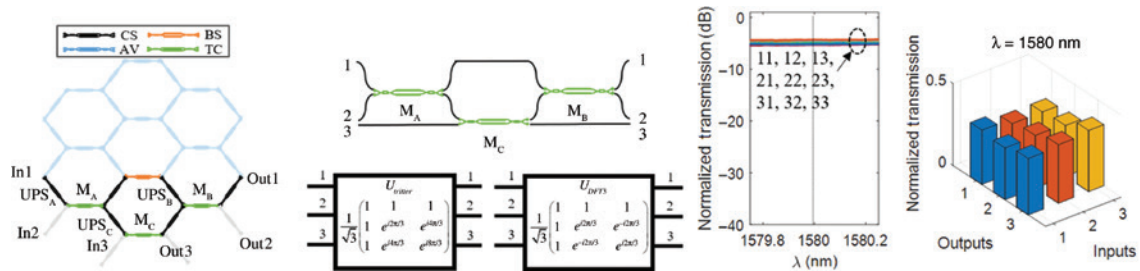

Figure 15: Unitary transformation configuration of a 3×3 interferometer based on a rectangular arrangement.
Left column: 7-cell configuration (CS = TBU in cross state, BS = MZI in bar state, TC = TBU in tunable coupler state, AV = TBU not employed); central-left column: circuit layout of the implemented interferometer; central-right column: spectral measurement of all input/output port connections; right column: normalized bar diagram of the resulting unitary matrix for $\lambda = 1580$ nm (after Ref. [15]).

5.2 Synthesis algorithms for SISO and 2×2 input/output circuits

The available synthesis methods for the specific hardware SISO and 2×2 configurations that can be emulated using the 2D integrated waveguide mesh can be applied by developing a suitable procedure, which translates the results provided by the synthesis equations into specific parameter values of the TBUs that are needed to implement the waveguide coupling points in the emulated layout. This is
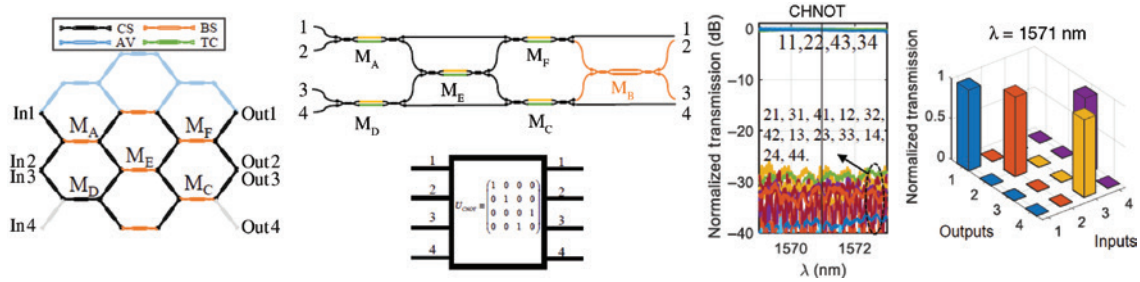
Figure 16: Programming and experimental results for a C-NOT transformation using the siicon waveguide mesh of Figure 9.
(A) Configuration of a 4×4 interferometer based on a rectangular arrangement to implement a C-NOT transformation; left column: 7-cell configuration (CS = MZI in cross state, BS = MZI in bar state, TC = MZI in tunable coupler state, AV = MZI not employed); central-left column: circuit layout of the implemented interferometer; central-right column: spectral measurement of all input/output port connections. Right column: normalized bar diagram of the resulting unitary matrix for $\lambda = 1571$ nm (after Ref. [15]).

Table 2: Circuit emulation capability of feedforward-only and feedforward/backward waveguide meshes.

	Feedforward-only waveguide meshes	Feedforward/backward waveguide meshes
Traditional FIR, IIR and FIR + IIR SISO and 2 × 2 filters	Only FIR	Yes
Multiport non-recirculating N×N Unitary Interferometers	Yes, but either triangular or rectangular depending on the configuration	Yes, both triangular and rectangular configurations
Multiport non-unitary M×N matrix transformers	Yes, but either triangular or rectangular depending on the configuration	Yes, both triangular and rectangular configurations
Multiport feedbackward subsytems	No	Yes

possible for all the main FIR, IIR and combined FIR + IIR discrete-time signal processing hardware configurations employed in practice. For example, FIR filters are based either on cascades/lattices of 3-dB tunable MZIs or in transversal filter configurations. For both FIR filter alternatives, synthesis and recursive scaling algorithms have been developed in the literature [34] directly applicable since the hexagonal waveguide mesh can directly implement both 3 dB-tuneable MZI cascade lattices and transversal filter configurations. For IIR filters, either simple/compound optical ring cavities of ring-loaded 3-dB tuneable MZI cascades are employed. Again, synthesis algorithms have been reported in the literature [34] that are directly applicable since the hexagonal waveguide mesh can directly implement either simple or multiple cavity ring filters or ring-loaded 3-dB tunable MZI cascades.

5.3 Synthesis algorithms for multiport non-recirculating N×N unitary interferometers

The 2D integrated waveguide mesh can emulate, as stated in Section 3, the two configurations for universal interferometers reported in the literature. This means that the detailed synthesis and recursive scaling algorithms, which have been developed by Miller [4] for triangular configurations [13] and by Clements et al. for rectangular

[14] configurations, can be applied provided that they are adapted to the hexagonal waveguide mesh configuration. These adaptations have been reported in the literature [12, 15, 23].

5.4 Synthesis algorithms for multiport non-recirculating M×N non-unitary interferometers

In a more general scope, the 2D integrated waveguide mesh can implement any singular value decomposition (SVD) of an $M \times N$ matrix D. The SVD states that an $M \times N$ matrix D can be decomposed as [4]:

$$D = VD_{diag}U^{\dagger} \qquad (2)$$

where U and V are $N \times N$ and $M \times M$ unitary matrices and D_{diag} is a $M \times N$ diagonal matrix. Figures 17 and 18 illustrate a 4×4 and 5×5 SVD transformation using the 2D hexagonal integrated waveguide mesh and the triangular and rectangular interferometer configuration, respectively.

5.5 Synthesis algorithms for multiport feedback and recirculating interferometers

Methods for synthesizing these structures have not yet been reported in the literature and are under current research.
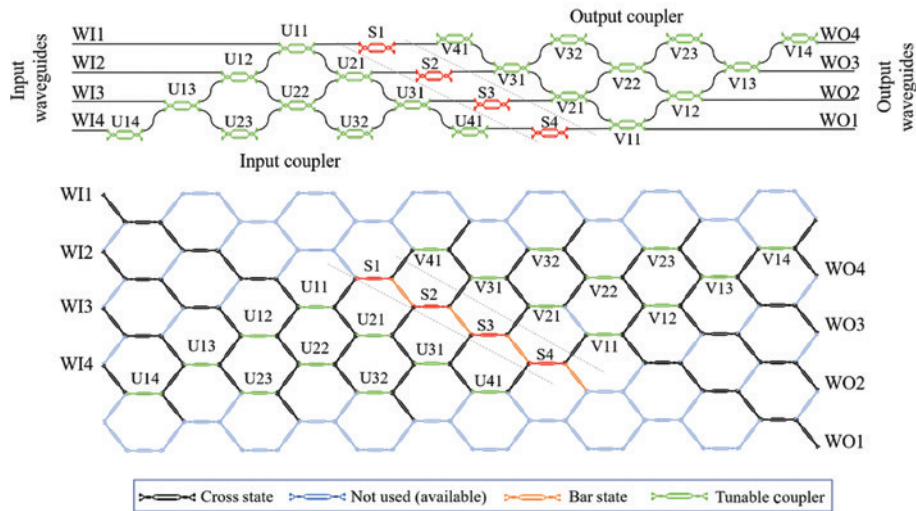
Figure 17: An example of the application of the singular value decomposition method to implement a universal non-unitary transformation emulated thorugh a triangular interferometer emulated by an hexagonal waveguide mesh.
Triangular interferometer layout (upper) and 2D hexagonal waveguide mesh implementation of a SVD for a 4×4 matrix transformation.
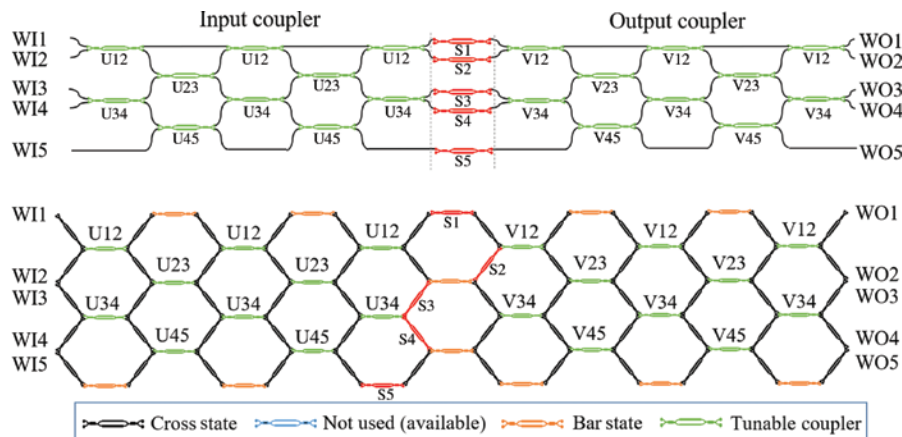

Figure 18: An example of the application of the singular value decomposition method to implement a universal non-unitary transformation emulated thorugh a rectangular interferometer emulated by an hexagonal waveguide mesh.
Rectangular interferometer layout (upper) and 2D hexagonal waveguide mesh implementation of a SVD for a 5×5 matrix transformation.

6 Current and future applications

PMIN based on 2D integrated feedforward/backward waveguide meshes can find applications in a myriad of new emerging fields as outlined in the introduction. *In the field of telecommunications and networking*, we have, for instance, provided a detailed discussion in Ref. [19] regarding their use in processor cores implementing the main required functionalities in microwave photonic systems and radio over fiber transmission. In particular, PMIN provides a potential alternative to a number of ASPICs that have been reported for delays lines [35, 36]. Tunable bandpass and notch filtering [37–47], reconfigurable signal processing [44–46], beamsteering [47–50], microwave

beamsplitters [51] and arbitrary radiofrequency waveform generators [52], to cite some examples. In all these applications, based on ultrafast implementations mainly using ring resonators, speed, bandwidth, tunability and footprint need to be optimal as outlined in several works [53–55]. The waveguide mesh concept fully addresses all of them. Furthermore, programmability allows not only for the structure reconfiguration but also for the fine tuning of circuit parameters in response to fabrication errors and time drifts.

This configuration can also emulate a triangular or rectangular multiport interferometer, which could be employed for mode unscrambling in a similar way to the configuration reported in Ref. [18]. Another interesting
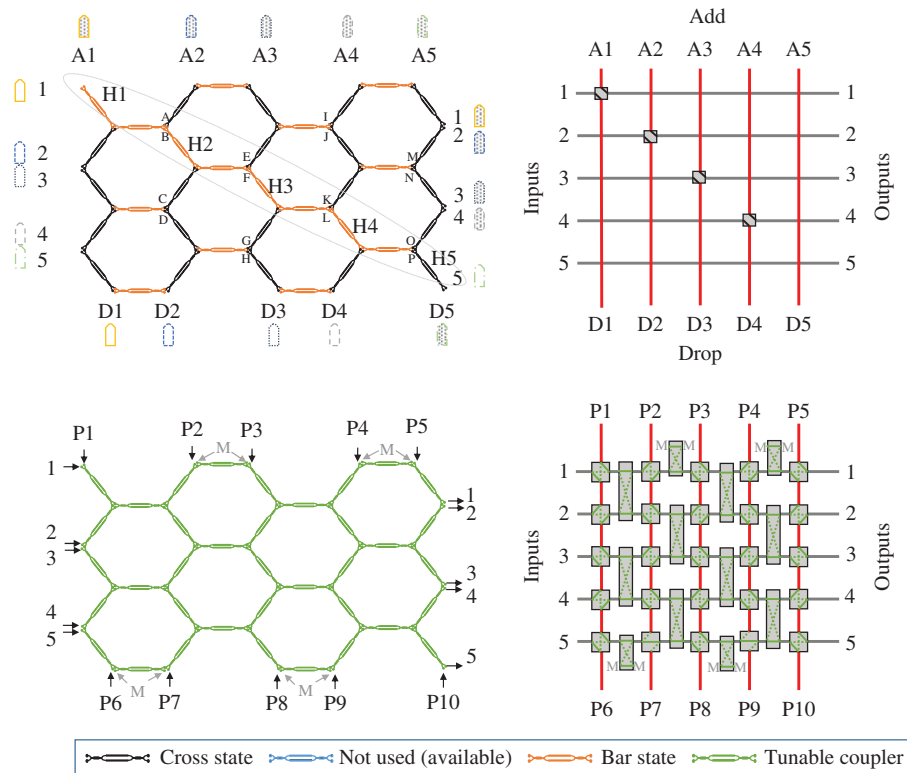
Figure 19: Waveguide mesh settings for channel management application: (upper) add-drop configurations for channels 1–4. Channel 5 bypasses the device. (Lower) Fully reconfigurable channel management station that allows channel broadcasting, add/drops, channel combinations and demultiplexing. *M*: signal monitoring points.

field of application is switching and interconnection [56, 57]. Hexagonal waveguide meshes emulating rectangular multiport interferometers can be programmed to manage different optical channels enabling broadcasting, add/ drop configurations, multiplexing and demultiplexing functions to cite but a few. A different device can be obtained if we add optical ports in not only the left and right side of the arrangement, but also in the top and bottom sides of the rectangular arrangement, a feature that is enabled by the hexagonal mesh topology. The main difference is that functionalities that are more compact can be achieved with this configuration. Consider that for the standard rectangular arrangement, add/drop functionality would require *N* input ports equal to the number of channel inputs (I) and add channels (A). In the same way, the number of output ports will be equal to the number of output channels (O) and drop channels (D).

Figure 19 (top) illustrates this new configuration that places add and drop channels in the upper and bottom part, respectively, enabling a more efficient device. The TBUs from H1 to H5 are set in bar state performing the add/drop operation for the matrix illustrated in Figure 19 (top/right). In particular, it corresponds to an add (drop) operation for A1(D1)–A4(D4) while channel 5 bypasses

the device. Figure 19 (lower) illustrates the fully reconfigurable interconnection matrix that can be programmed. Each block is a tunable coupler and can be configured as a switch or define a desired splitting ratio in order to enable broadcasting, multiplexing, demultiplexing or switching operations.

The implementation of arbitrary unitary matrices enables the emulation of any linear transformation, which is a fundamental operation in many other fields of application. For instance, in the area of *Quantum Information*, $N \times N$ unitary transformations support the implementation of simple and complex logic gates [58–64], the emulation of boson sampling [65–67] circuits and quantum lab on a chip [68], to cite a few applications. Waveguide meshes open the path for reconfigurable large-scale integrated quantum information systems with a potential to superseed current approaches based on static configurations [69]. Furthermore, since meshes can be implemented in completely symmetric configurations they naturally enable reversible operation, which is essential for quantum information processing. In *Computer processor Interconnections*, reconfigurable broadband inter-processor and computer interconnections are fundamental in high-performance computing and data centers [70].

Photonic linear transformations provide a clean, interference-free and high-speed option for core processor resource management [71]. In the field of *Optical Signal processing*, linear transformations that can be supported by PMIN processors based on 2D waveguide meshes include several operations that are central to optical signal processing as, for example: the Optical FFT [72], Hilbert transformation [73], Integrators and differentiators [74, 75]. In *Neurophotonics*, unitary ($N \times M$) and non-unitary ($N \times M$) Matrix transformations are fundamental building blocks preceding non-linear threshold operations in neural networks, spike and reservoir computing [76, 77]. The availability of PMIN processors opens an interesting and exciting research avenue in this emerging field. In the area of *Biophotonic Sensors*, PMINs support simple and MIMO interferometric structures for lab-on-a-chip and multiparameter sensing applications enable the future implementation of multiparameter integrated photonic sensing [78, 79]. Finally, but not least important, in *Advanced Physics* waveguide mesh PMIN provides a programable 2D platform to implement different topological systems such as multi-ring cavity structures to support research in synthetic dimensions and devices based on topological insulator principles [80–82].

7 Summary, conclusions and future work

We have reviewed the recent advances reported in the field of programmable multifunctional nanophotonic circuits implemented by means of integrated waveguide meshes, both from the theoretical as well as from the experimental point of view. We have shown how these devices can be programmed to implement both traditional signal processing structures, such as finite and infinite impulse response filters, delay lines, beamforming networks as well as more advanced linear matrix optics functionalities. It is in this latter topic, where the true potential of 2D integrated waveguide meshes for the implementation of complex configurations, supporting linear matrix transformations, needs still to be unleashed. The first results indicate that these structures can be able to support basically any $N \times N$ unitary transformation by emulation of previously reported multiport interferometers and, moreover, non-unitary $N \times M$ transformations can be supported by suitable translation of the results of the singular value decomposition technique into the mesh structure.

Several issues need to be addressed in order to enable the implementation of structures featuring higher-order complexity. From the practical point of view, a higher degree of complexity means a higher number of cells implemented in the low footprint available substrate. This entails several trade-offs. On one hand, the TBU length must be reduced and this in turn puts pressure into the available tuning mechanisms, as thermal tuning requires a minimum electrode length. The solution to this problem calls for researching other tuning mechanisms possibly based on plasma dispersion effect [83] or in piezo and optomechanical effects [84]. On the other hand, a higher number of cells mean higher propagation and insertion losses, and this will at a given point require the use of semiconductor optical amplifiers (SOAs). Work needs to be carried to determine the optimum SOA allocation within the waveguide mesh and, most probably, will require the hosting of these devices outside the mesh in special amplification tiers. Another practical issue is the control of the TBU bias points within the mesh in real time. Several techniques and methods have been proposed [6, 85] and that based on non-invasive techniques (CLIPP), Ref. [85] is especially attractive. Nevertheless, with the increase in complexity and the number of elements to be controlled, these approaches may not even render practical. One possible approach to overcome this limitation can be resorting to the incorporation of machine learning techniques [86], which can enable an initial training stage of the waveguide mesh and subsequent monitoring just by analizing its output port signals.

The versatility of mesh-based PMIN processors is directly proportional to the number of integrated TBUs. However, the scalability of these systems is limited by different factors: TBU insertion loss, power consumption, optical crosstalk/signal leakage, footprint and the complexity of their control electronics.

From these, the dominant limit is the insertion loss of the TBU, which is mainly generated by the inner coupling structures and phase-tuning mechanisms. In order to compare them with conventional PICs, we can decouple the total insertion loss per TBU as the sum of the propagation loss and the additional losses (beamsplitters and tuning mechanism). Even using state-of-the-art beamsplitters and fabrication procedures, going below 0.2-dB additional loss per TBU is a current challenge. With these numbers, we can estimate that a programmed light path of 50 TBUs introduce 10-dB additional loss, setting a scalability limit of the size of the programmed circuits and a TBU miniaturization trade-off [19].

Regarding the power consumption ($P_{\pi TBU}$), exploring alternative tuning mechanism approaches will be fundamental to find power-efficient, low-loss, reduced-size, focalized and low-crosstalk phase shifters. In this sense,

thermal tuners have been optimized in the last years to open the path for either sub-miliWatts power consumptions [87] or reduced footprint structures [33]. For a mesh of N TBUs, the average power consumption is less than $N \cdot P_{\pi TBU}$. In addition, low-loss alternatives enabling an increase in the tuning speed tuners would open the path to a wider range of application in optical/quantum information processing.

An additional concern is related to non-desired side effects arising from the use of non-ideal components. For example, optical crosstalk due to the drift in the configured coupling value and to fabrication or design errors. The optical crosstalk produces signal leaking through the overall mesh that causes reflections inside the circuits, creating ripples in the spectral response and even lasing phenomena [23]. This issue has been addressed for feedforward meshes by Miller [6] and for feedforward/feedbackward operations in Ref. [12]. In the context of waveguide meshes, the unused TBUs can be smartly configured to extract the leaked signal to drain optical ports to radically improve the system performance and relax the TBU specifications to optical crosstalk levels below 20 dB to assure a good circuit performance.

If ultra-low-loss, low-power TBUs are obtained, future mesh-based PMIN circuits will require an increment of the integration densities to further enlarge their performance in a similar way as the number of transistors per chip rate rises in electronic processors. To overcome the TBU miniaturization trade-offs, three-dimensional (3D) Si photonic platforms can be considered [88]. The implementation of feed-forward waveguide mesh 3D approaches has been addressed in Ref. [89], where termed *Fast* implementations are trade-off against the planar 2D implementations based on the triangular [13] and rectangular [14] approaches. The main conclusion is that proposed 3D approaches do not seem to compare favorably as they do not sustain universal linear transformations in general (see table in Figure 1 in Ref. [89]). In a similar way, schemes based on photonic crystals, metamaterials and plasmonic effects are not yet competitive. The engineering of these devices is still focused on simple components and complex multifunctional structures for which multiple signal control mechanisms that need to be employed have not yet been considered. In these platforms and especially in those based on photonic crystals, phase tuning based on non-linear effects might be an option, but controllable and repeatable tuning schemes have not been reported so far that rely on low power consumption.

In parallel, a considerable effort is being developed in the co-package stage for the subsystems enabling the control electronics for PICs with a large number of independent electrical channels. These are typically FPGA/DSP driven solutions [30], ASIC approaches [90] and more recently, fully-integrated solutions of photonic/electronics in the same substrate [91].

From the theoretical point of view, there are two main issues to be addressed. The first one is the development of a technique for the full analysis of these structures, which can render any input/output port transfer function and is scalable, that is, independent of the number of cells in the waveguide mesh. This question is under current investigation by our group. The second issue is connected to the need of developing a synthesis procedure for the implementation of multiport feedback and recirculating interferometers by emulation in the waveguide mesh. Yet the 2D structures might also provide their own implementation of the above transformations without requiring the circuit emulation. Future work should be directed towards this exciting area of research.

If the above issues are correctly addressed, PMIN processors will enable an impressive number of known and future application fields.

References

[1] Peruzzo A, Laing A, Politi A, Rudolph T, O'Brien JL. Multimode quantum interference of photons in multiport integrated devices. Nat Commun 2011;2:224.

[2] Metcalf BJ, Thomas-Peter N, Spring JB, et al. Multiphoton quantum interference in a multiport integrated photonic device. Nat Commun 2013;4:1356.

[3] Miller DAB. Self-aligning universal beam coupler. Opt Express 2013;21:6360–70.

[4] Miller DAB. Self-configuring universal linear optical component. Photon Res 2013;1:1–15.

[5] Carolan J, Harrold C, Sparrow C, et al. Universal linear optics. Science 2015;349:711.

[6] Miller DAB. Perfect optics with imperfect components. Optica 2015;2:747–50.

[7] Harris NC, Steinbrecher GR, Prabhu M, et al. Quantum transport simulations in a programmable nanophotonic processor. Nat Photon 2017;11:447–52.

[8] Graydon O. Birth of the programmable optical chip. Nat Photon 2016;10:1.

[9] Zhuang L, Roeloffzen CGH, Hoekman M, Boller KJ, Lowery AJ. Programmable photonic signal processor chip for radiofrequency applications. Optica 2015;2:854–9.

[10] Pérez D, Gasulla I, Capmany J, Soref RA. Reconfigurable lattice mesh designs for programmable photonic processors. Opt Express 2016;24:12093–106.

[11] Capmany J, Gasulla I, Pérez, D. Microwave photonics: the programmable processor. Nat Photon 2016;10:6–8.

[12] Pérez D, Gasulla I, Crudgington L, et al. Multipurpose silicon photonics signal processor core. Nat Commun 2017;8:636.

[13] Reck M, Zeilinger A, Bernstein HJ, Bertani P. Experimental realization of any discrete unitary operator. Phys Rev Lett 1994;73:58–61.

[14] Clements WR, Humphreys PC, Metcalf BJ, Steven Kolthammer W, Walmsley IA. Optimal design for universal multiport interferometers. Optica 2016;3:1460–5.

[15] Pérez D, Gasulla I, Fraile FJ, et al. Silicon photonics rectangular universal interferometer. Lasers Photon Rev 2017;11:1700219.

[16] Shen Y, Harris NC, Skirlo S, et al. Deep learning with coherent nanophotonic circuits. Nat Photon 2017;11:441–6.

[17] Ribeiro A, Ruocco A, Vanacker L, Bogaerts W. Demonstration of a 4×4-port universal linear circuit. Optica 2016;3:1348–57.

[18] Anoni A, Guglielmi E, Carminati M, et al. Unscrambling light – automatically undoing strong mixing between modes. Light Sci Appl 2017;6:e17110.

[19] Capmany J, Gasulla I, Pérez D. Towards programmable microwave photonics processors. IEEE J Lightwave Tech 2018;26:519–32.

[20] Chen L-N, Hall E, Theogarajan L, Bowers J. Photonic switching for data center applications. IEEE Photon J 2011;3:834–44.

[21] Miller DAB. Silicon photonics: meshing optics with applications. Nat Photon 2017;11:403–4.

[22] Thomas-Peter N, Langford NK, Datta A, et al. Integrated photonic sensing. New J Phys 2011;13:055024.

[23] Pérez D. Integrated Microwave Photonic Processors using Waveguide Mesh Cores, PhD Thesis. Universitat Politècnica de València, 2017.

[24] Pérez D, Sánchez E, Capmany J. Programmable True-Time Delay Lines using integrated waveguide meshes. IEEE J Lightwave Tech 2018, in press.

[25] Mower J, Harris NC, Steinbrecher GR, Lahini Y, Englund D. High-fidelity quantum state evolution in imperfect photonic integrated circuits. Phys Rev. A 2015;92:032322.

[26] Corbett B, Loi R, Zhou W, Liu D, Ma Z. Transfer print techniques for heterogeneous integration of photonic components. Prog Quantum Electron 2017;52:1–17.

[27] Van der Tol JGM, Jiao Y, Shen L, et al. Indium Phosphide Integrated Photonics in Membranes. IEEE J Sel T Quantum Electron 2018;24:6100809.

[28] Harris N, Steinbrecher GR, Prabhu M, et al. Quantum transport simulations in a programmable nanophotonic processor. Nat Photon 2017;11:447–53.

[29] Micó G, Bru L, Pastor D, et al. C-band linear propagation properties for a 300 nm film height Silicon Nitride photonics platform. European Conference on integrated optics 2017: Eindhoven, Netherlands, 2017.

[30] Celo D, Goodwill DJ, Jiang J, et al. 32×32 silicon photonic switch. OptoElectronics and communications conference & IEEE Photonics in Switching, Niigata, Japan, 2016.

[31] Sheng Z, Wang Z, Qiu C, et al. A compact and low-loss MMI coupler fabricated with CMOS Technology. IEEE Photon J 2012;4:22272–7.

[32] Cong GW, Suzuki K, Kim SH, Tanizawa K, Namiki S, Kawashima H. Demonstration of a 3-dB directional coupler with enhanced robustness to gap variations for silicon wire waveguide. Opt Express 2014;22:2051–9.

[33] Harris NC, Ma Y, Mower J, et al. Efficient, compact and low loss thermos-optic phase shifter in silicon. Opt Express 2014;22:10487–93.

[34] Madsen CK, Zhao JH. Optical filter design and analysis: a signal processing approach. New York, USA, John Wiley & Sons Inc., 1999.

[35] Zhuang L, Marpaung D, Burla M, Beeker W, Leinse A, Roeloffzen C. Low-loss, high-index-contrast Si3N4/SiO2 optical waveguides for optical delay lines in microwave photonics signal processing. Opt Express 2011;19:23162–70.

[36] Burla M, Marpaung D, Zhuang L, et al. On-chip CMOS compatible reconfigurable optical delay line with separate carrier tuning for microwave photonic signal processing. Opt Express 2011;19:21475–84.

[37] Zhuang L, Hoekman M, Beeker W, et al. Novel low-loss waveguide delay lines using Vernier ring resonators for on-chip multi-λ microwave photonic signal processors. Laser Photon Rev 2013;7:994–1002.

[38] Choudhary A, Aryanfar I, Shahnia S, et al. Tailoring of the Brillouin gain for on-chip widely tunable and reconfigurable broadband microwave photonic filters. Opt Lett 2016;41:436–9.

[39] Tu KY, Rasras MS, Gill DM, et al. Silicon RF-photonic filter and down-converter. J Lightwave Technol 2010;28:3019–28.

[40] Fandiño JS, Muñoz P, Doménech D, Capmany J. A monolithic integrated photonic microwave filter. Nat Photon 2017;11:124–9.

[41] Rasras MS, Tu KY, Gill DM, et al. Demonstration of a tunable microwave-photonic notch filter using low-loss silicon ring resonators. J Lightwave Technol 2009;27:2105–10.

[42] Sancho J, Bourderionnet J, Lloret J, et al. Integrable microwave filter based on a photonic crystal delay line. Nat Commun 2012;3:1075.

[43] Orlandi P, Morichetti F, Strain MJ, Sorel M, Bassi P, Melloni A. Photonic integrated filter with widely tunable bandwidth. J Lightwave Technol 2014;32:897–907.

[44] Norberg EJ, Guzzon RS, Nicholes SC, Parker JS, Coldren LA. Programmable photonic lattice filters in InGaAsP-InP. IEEE Photon Technol Lett 2010;22:109–11.

[45] Guzzon RS, Norberg EJ, Parker JS, Johansson LA, Coldren LA. Integrated InP-InGaAsP tunable coupled ring optical bandpass filters with zero insertion loss. Opt Express 2011;19:7816–26.

[46] Liu W, Li M, Guzzon RS, et al. A fully reconfigurable photonic integrated signal processor. Nat Photon 2016;10:190–5.

[47] Roeloffzen C, Oldenbeuving R, Timens RB, et al. Integrated optical beamformers. Optical Fiber Communication Conference 2015: Los Angeles, CA, USA, ThA2, 2015.

[48] Zhuang L, Roeloffzen CGH, Heideman RG, Borreman A, Meijerink A, Etten WV. Single-chip ring resonator-based 1×8 optical beam forming network in CMOS-compatible waveguide technology. IEEE Photon Technol Lett 2007;19:1130–2.

[49] Zhuang L, Hoekman M, Taddei C, et al. On-chip microwave photonic beamformer circuits operating with phase modulation and direct detection. Opt Express 2014;22:17079–91.

[50] Burla M, Marpaung DAI, Zhuang L, et al. Multiwavelengthintegrated optical beamformer based on wavelength división multiplexing for 2-D phased array antennas. J Lightwave Technol 2014;32:3509–20.

[51] Zhuang L, Burla M, Taddei C, et al. Integrated microwave photonic splitter with reconfigurable amplitude, phase, and delay offsets. Opt Lett 2015;40:5618–21.

[52] Wang J, Shen H, Fan L, et al. Reconfigurable radio-frequency arbitrary waveforms synthesized in a silicon photonic chip. Nat Commun 2015;6:5957.

[53] Agarwal A, Toliver P, Menendez R, et al. Fully programmable ring-resonator-based integrated photonic circuit for phase coherent applications. IEEE J Lightwave Tech 2006;24:77–87.

[54] Sethi P, Roy S. Ultrafast all-optical flip-flops, simultaneous comparator-decoder and reconfigurable logic unit with silicon microring resonator switches. IEEE J Sel Top Quantum Electron 2014;20:5900308.

[55] Sethi P, Roy S. All-optical ultrafast switching in 2×2 silicon microring resonators and its application to reconfigurable DEMUX/MUX and reversible logic gates. IEEE J Lightwave Tech 2014;32:2173–80.

[56] Bergman K. Silicon Photonics For High Performance Interconnection Networks. in Optical Fiber Communication Conference, OSA Technical Digest (online) (Optical Society of America, (2018), Tu3F.1.

[57] Soref R. Integrated-photonic switching structures. Appl Phys Lett Photon 2018;3:021101.

[58] Knill E, Laflamme R, Milburn GJ. A scheme for efficient quantum computation with linear optics. Nature 2001;409:46–52.

[59] Kok P, Munro WJ, Nemoto K, Ralph TC, Dowling JP, Milburn GJ. Linear optical quantum computing with photonic qubits. Rev Mod Phys 2007;79:135–74.

[60] O'Brien JL, Furusawa A, Vučković J. Photonic quantum technologies. Nat Photon 2009;3:687–95.

[61] Thompson MG, Politi A, Matthews JC, O'Brien JL. Integrated waveguide circuits for optical quantum computing. IET Circuits Devices Syst 2011;5:94–102.

[62] Politi A, Matthews J, Thompson M, O'Brien J. Integrated quantum photonics. IEEE J Select Top Quantum Electron 2009;15:1673–84.

[63] Politi A, Cryan MJ, Rarity JG, Yu S, O'Brien JL. Silica-on-silicon waveguide quantum circuits. Science 2008;320:646–9.

[64] Kieling K, O'Brien JL, Eisert J. On photonic controlled phase gates. New J Phys 2010;12:013003.

[65] Spring JB. Metcalf BJ, Humphreys PC, et al. Boson sampling on a photonic chip. Science 2013;339:798–801.

[66] Broome MA, Fedrizzi A, Rahimi-Keshari S, et al. Photonic boson sampling in a tunable circuit. Science 2013;339:794–8.

[67] Crespi A, Osellame R, Ramponi R, et al. Integrated multimode interferometers with arbitrary designs for photonic boson sampling. Nat Photon 2013;7:545–9.

[68] Lanyon BP, Whitfield JD, Gillett GG, et al. Towards quantum chemistry on a quantum computer. Nat Chem 2010;2:106–11.

[69] Harris N, Bunandar D, Pant M, et al. Large-scale quantum photonic circuits in silicon. Nanophotonics 2016;5:456–68.

[70] Shen Y, Hattink MHN, Samadi P, et al. Software-defined networking control plane for seamless integration of multiple silicon photonic switches in Datacom networks. Opt Express 2018;26:10914–29.

[71] Sun C, Wade MT, Lee Y, et al. Single-chip microprocessor that communicates directly using light. Nature 2015;528:534–8.

[72] De Chatellus HG, Cortés LR, Azaña J. Optical real-time Fourier transformation with kilohertz resolutions. Optica 2016;3:1–8.

[73] Zhuang L, Khan MR, Beeker W, Leinse A, Heideman R, Roeloffzen C. Novel microwave photonic fractional Hilbert transformer using a ring resonator-based optical all-pass filter. Opt Express 2012;20:26499–510.

[74] Taddei C, Yen NTH, Zhuang L, et al. Waveguide filter-based on-chip differentiator for microwave photonic signal processing. IEEE International Topical Meeting on Microwave Photonics 2013: Alexandria, VA, USA, 2013:28–31.

[75] Ferrera M, Park Y, Razzari L, et al. On-chip CMOS-compatible all-optical integrator. Nat Commun 2010;1:29.

[76] Shen Y, Harris NC, Skirlo S, et al. Deep learning with coherent nanophotonic circuits, Nat Photon 2017;11:441–7.

[77] Pengy HT, Nahmiasy MA, Ferreira de Lima T, Tait AN, Shastri BJ, Prucnal PR. Neuromorphic Photonic Integrated Circuits. IEEE J Sel Topics Quant Electron. In press.

[78] Estevez MC, Alvarez M, Lechuga L. Integrated optical devices for lab-on-a-chip biosensing applications. Laser Photon Rev 2012;6:463–87.

[79] Heideman R, Hoekman M, Schreuder E. TriPleX-based integrated optical ring resonators for lab-on-a-chip and environmental detection. IEEE J Sel Topics Quant Electro 2012;18:1583–96.

[80] Ozawa T, Price HM, Goldman N, Zilberberg O, Carusotto I. Synthetic dimensions in integrated photonics: From optical isolation to four-dimensional quantum Hall physics. Phys Rev A 2016;93:043827.

[81] Harari G, Bandres MA, Lumer Y, et al. Topological insulator laser: theory. Science 2018;359. DOI: 10.1126/science.aar4003.

[82] Bandres MA, Wittek S, Harari G, et al. Topological insulator laser: experiments. Science 2018;359. DOI: 10.1126/science.aar400.

[83] Soref R, Bennett B. Electrooptical effects in silicon. IEEE J of Quant Electron 1987;23:123–9.

[84] Hosseini N, Dekker R, Hoekman M, et al. Stress-optic modulator in TriPleX platform using a piezoelectric lead zirconate titanate (PZT) thin film. Opt Express 2015;23:14018–26.

[85] Grillanda S, Carminati M, Morichetti F, et al. Non-invasive monitoring and control in silicon photonics using CMOS integrated electronics. Optica 2014;1:129–36.

[86] Zibar D, Piels M, Jones R, Schäeffer CG. Machine learning techniques in optical communication. J Lightwave Technol 2016;34:1442–52.

[87] Fang Q, Song JF, Liow T-Y, et al. Ultralow power silicon photonics thermo-optic switch with suspended phase arms. IEEE Photon Technol Lett 2011;23:525–7.

[88] Wesley D, Mikkelsen JC, Dumais P, et al. Tri-layer silicon nitride-on-silicon photonic platform for ultra-low-loss crossings and interlayer transitions. Opt Express 2017;25:30862–75.

[89] Flamini F, Spagnolo N, Viggianiello N, Crespi A, Osellame R, Sciarrino F. Benchmarking integrated linear optical architectures for quantum information processing. Sci Rep 2017;7:715133.

[90] Annoni A, Guglielmi E, Carminati M, et al. Automated routing and control of silicon photonic switch fabrics. IEEE Journal of Sel Topics in Quantum Electron 2016;22:169–76.

[91] Atabaki AH. Integrating photonics with silicon nanoelectronics for the next generation of systems on a chip. Nature 2018;556:349–54.